Darren C. Henstridge,[1] Clinton R. Bruce,[1,2] Brian G. Drew,[3] Kálmán Tory,[4] Attila Kolonics,[4] Emma Estevez,[1] Jason Chung,[1] Nadine Watson,[1] Timothy Gardner,[1] Robert S. Lee-Young,[1] Timothy Connor,[5] Matthew J. Watt,[2] Kevin Carpenter,[6] Mark Hargreaves,[7] Sean L. McGee,[5] Andrea L. Hevener,[3] and Mark A. Febbraio[1,4]

Activating HSP72 in Rodent Skeletal Muscle Increases Mitochondrial Number and Oxidative Capacity and Decreases Insulin Resistance

Diabetes 2014;63:1881–1894 | DOI: 10.2337/db13-0967

Induction of heat shock protein (HSP)72 protects against obesity-induced insulin resistance, but the underlying mechanisms are unknown. Here, we show that HSP72 plays a pivotal role in increasing skeletal muscle mitochondrial number and oxidative metabolism. Mice overexpressing HSP72 in skeletal muscle (HSP72Tg) and control wild-type (WT) mice were fed either a chow or high-fat diet (HFD). Despite a similar energy intake when HSP72Tg mice were compared with WT mice, the HFD increased body weight, intramuscular lipid accumulation (triacylglycerol and diacylglycerol but not ceramide), and severe glucose intolerance in WT mice alone. Whole-body VO_2, fatty acid oxidation, and endurance running capacity were markedly increased in HSP72Tg mice. Moreover, HSP72Tg mice exhibited an increase in mitochondrial number. In addition, the HSP72 coinducer BGP-15, currently in human clinical trials for type 2 diabetes, also increased mitochondrial number and insulin sensitivity in a rat model of type 2 diabetes. Together, these data identify a novel role for activation of HSP72 in skeletal muscle. Thus, the increased oxidative metabolism associated with activation of HSP72 has potential clinical implications not only for type 2 diabetes but also for other disorders where mitochondrial function is compromised.

Although obesity is associated with insulin resistance, the exact mechanism by which increased adiposity contributes to this disorder is unresolved. It is well established, however, that insulin resistance is associated with excess ectopic expression of lipid in liver and skeletal muscle (1). Moreover, the accumulation of deleterious lipid species such as diacylglycerol (DAG) (2,3) and ceramide (4) is known to impair insulin action. Apart from the role of excess ectopic lipid accumulation, it has become apparent that insulin resistance may also be associated with defective oxidative metabolism in skeletal muscle (5). A coordinated reduction in the expression of genes encoded by peroxisome proliferator–activated receptor (PPAR) γ coactivator (PGC)-1α is observed in skeletal muscle of patients with type 2 diabetes (6,7) and healthy subjects with a family history of diabetes (7). In addition, mitochondrial function in skeletal muscle plays a vital role in the pathogenesis of type 2 diabetes (8,9). Importantly, activation of key pathways involving AMP-activated protein kinase (AMPK) (10), PPARδ (11), sirtuin 1 (SIRT)1 (12), and

[1]Cellular and Molecular Metabolism Laboratory, Baker IDI Heart and Diabetes Institute, Melbourne, Victoria, Australia
[2]Department of Physiology, Monash University, Clayton, Victoria, Australia
[3]Division of Endocrinology, Diabetes and Hypertension, David Geffen School of Medicine, University of California, Los Angeles, Los Angeles, CA
[4]N-Gene Research Laboratories, Inc., Budapest, Hungary
[5]Metabolic Research Unit, School of Medicine, Deakin University, Geelong, Victoria, Australia
[6]Department of Biochemical Genetics, Children's Hospital at Westmead and Disciplines of Genetic Medicine and Paediatrics and Child Health, University of Sydney, New South Wales, Australia
[7]Department of Physiology, University of Melbourne, Parkville, Victoria, Australia

Corresponding author: Mark A. Febbraio, mark.febbraio@bakeridi.edu.au.

Received 19 June 2013 and accepted 9 January 2014.

This article contains Supplementary Data online at http://diabetes.diabetesjournals.org/lookup/suppl/doi:10.2337/db13-0967/-/DC1.

D.C.H. and C.R.B. contributed equally to this study.

carnitine palmitoyltransferase-1 (CPT1) (13) increase fatty acid oxidation (FAO), thereby decreasing lipid esterification, and in so doing, ameliorate insulin resistance. Hence, activators of these pathways are thought to have therapeutic potential for the treatment of type 2 diabetes.

We have identified an essential role for heat shock protein (HSP)72 (the inducible form of the 70-kDa family of HSPs) in preventing insulin resistance in the context of high-fat feeding or genetic obesity in mice (14). In this (14) and subsequent (15,16) studies, overexpression of HSP72 was accompanied by a marked reduction in high-fat diet (HFD)-induced activation of proinflammatory signaling, i.e., phosphorylation of c-Jun *N*-terminal kinase (p-JNK) in skeletal muscle, which is implicated in insulin resistance (17). However, whether this decrease in p-JNK could account for all of the whole-body protective effects of HSP72 overexpression is debatable. Since HSP72 transgenic mice are protected from developing obesity in the absence of hyperphagia, it is possible that they have increased energy expenditure (14). In addition, markers of oxidative metabolism in skeletal muscle are increased in HSP72 transgenic (HSP72Tg) mice (14) and in C2C12 muscle cells (18) and rats (15) undergoing heat treatment to induce HSP72. These data are in agreement with our previous observations that correlate increased HSP72 expression with mitochondrial enzyme activity in human skeletal muscle (19). Together, these studies raise the hypothesis that the mechanism of HSP72 action may be in regulating energy balance via enhanced oxidative metabolism in skeletal muscle. To test this hypothesis, we fed HSP72Tg and control mice either a standard chow diet or HFD. We also treated type 2 diabetic (Goto-Kakizaki [GK]) rats with the HSP72 coinducer BGP-15, currently in human clinical trials for type 2 diabetes (20). In both experimental models, overexpression or induction of HSP72 increased mitochondrial number.

RESEARCH DESIGN AND METHODS

Mouse Studies

Male wild-type (WT) and HSP72Tg mice were used as previously reported (14). In addition, for testing of whether the HSP72Tg phenotype was penetrative across different genetic strains of mice, additional studies were performed in HSP72Tg and littermate control mice, back-crossed at least 10 times onto a C57BL/6 background. All experiments were approved by the Alfred Medical Research Education Precinct Animal Ethics Committee. All experiments commenced when mice were 8 weeks of age. Mice were fed either a chow diet (5% of total energy from fat) or an HFD (45% of total energy from fat) for 10 weeks. Animals were given their prescribed diet and water ad libitum and housed in a controlled environment with a 12-h light-dark cycle.

Glucose Tolerance Test and Analysis of Insulin Signaling and Insulin-Stimulated Glucose Clearance

Glucose tolerance tests (1g/kg i.p.) were performed in 5-h fasted mice as previously described (21). Insulin-stimulated glucose clearance was examined as previously described (22). The rate of tissue metabolism of [^{3}H]2-deoxy-D-glucose was calculated by use of the single-injection model (23).

Euglycemic-Hyperinsulinemic Clamp

Male Goto-Kakizaki rats weighing 200–250 g were treated with daily oral doses of BGP-15 (5, 10, 20, and 30 mg/kg), rosiglitazone (2 mg/kg), metformin (100 mg/kg), or vehicle for five days. Insulin sensitivity was evaluated on the fifth day 4–6 h after the last treatment by hyperinsulinemic-euglycemic clamp method. Animals were anesthetized with thiopental sodium. Venous catheters were placed in the external jugular veins for insulin and glucose administration. An arterial cannula was inserted into the right carotid artery for arterial blood glucose measurement. Human regular insulin was infused at a constant rate (13 mU/kg/min; Novo Nordisk, Copenhagen) over 120 min. Blood samples were taken from the arterial cannula for blood glucose concentration measurements at 5-min intervals. Blood glucose concentration was maintained constant (5.5 $\pm$ 0.5 mmol/L) by variable rate of glucose infusion via the venous cannula. When glucose infusion stabilized for at least 20–30 min, we defined the condition as steady state. The glucose infusion rate (mg/kg/min) during the steady state was used to characterize insulin sensitivity.

Indirect Calorimetry and Exercise Tests

VO_2 was measured using a 12-chamber indirect calorimeter (Oxymax series; Columbus Instruments, Columbus, OH) with an airflow of 0.6 L/min as previously described (24). For exercise tests, mice were subjected to a 3-day familiarization protocol that consisted of progressively increasing the intensity and duration of treadmill running (Columbus Instruments, Columbus, OH) before experimental testing. All experiments were performed at 1000 h, and food was withdrawn from mice 4 h prior to running. Mice performed two exercise tests separated by 3 days. Initially, an incremental exercise test was performed that consisted of mice running at 10 m/min for 2 min. The velocity was increased by 2 m/min every 2 min. Once treadmill speed reached 20 m/min, the gradient was increased by 5% every 2 min until fatigue. This was defined as spending $>$10 s at the base of the treadmill despite manual encouragement. Three days later, endurance capacity was assessed by running mice at 16 m/min at a 5% grade until they reached fatigue.

Ex Vivo Muscle Incubations

For palmitate activation of JNK experiments, soleus muscles from WT or HSP72Tg mice were carefully dissected tendon to tendon and placed in sealed flasks containing pregassed (95% O_2/5% CO_2) Krebs-Henseleit buffer, pH 7.3, supplemented with 4% BSA and 4 mmol/L pyruvate. Muscles were allowed to recover for 30 min and were incubated with 0.5 mmol/L or 1.5 mmol/L palmitic acid for 6 h. Palmitate oxidation studies were performed as previously described (25)

Western Blotting

Muscle samples were lysed and protein concentration was determined as previously described (26). Immunoblotting was performed using the following primary antibodies: pAkt Ser^{473}, pAkt Thr^{308}, total Akt, pSAPK/JNK Thr^{183}/Tyr^{185}, total JNK, SIRT1 (mouse specific), acetylated Lys, parkin, LC3, ATG12, PKC-α, PKC-δ, and PKC-θ (Cell Signaling); lipoprotein lipase (LPL) (Abcam); CD36 (R&D Systems); p62 (ProGen); PINK1 (Cayman Chemicals); PGC-1α (Millipore); and α-tubulin (Sigma-Aldrich). For protein kinase C (PKC) studies, subcellular fractionation was carried out as previously described (13).

RNA Extraction and Real-Time Quantitative PCR

Total RNA was isolated from skeletal muscle tissue with Tri Reagent (Sigma Aldrich) and reverse transcribed to cDNA with the use of random hexamers. Real-time PCR was performed on a 7500 fast sequence detector (Applied Biosystems). Each assay included a no-template control and a no-reverse transcriptase control. Oligos for PGC-1α (Mm01208835_m1), SIRT1 (Mm00490758_m1), mitochondrial transcription factor A (Tfam) (Mm00447485_m1), CD36 (Mm01135198_m1), CPT1b (Mm00487200m1), FABPpm (Mm02342495_m1), HSL (Mm00495359_m1), LPL (Mm00434770), nuclear respiratory factor 1 (Mm00447996_m1), FATP1 (Mm00449511_m1), ATGL1 (Pnpla2) (Mm00503040_m1), DGAT1 (Mm00515643_m1), and DGAT2 (Mm00499536_m1) were obtained from Applied Biosystems, TaqMan. Cyclophilin A (forward, aggatgagaacttcatcctgaagc; reverse, ttggcagtgcagataaaaaactg) was from Geneworks. The relative concentrations of measured mRNAs were determined by plotting the threshold cycle (C_t) versus the log of the serial dilution points, and the relative expression of the gene of interest was determined after normalization to 18S or cyclophilin A.

Muscle Metabolites and Enzymes

Triacylglycerol (TAG), DAG, and ceramide content were determined in the quadriceps muscles using methods previously described (13,21). Citrate synthase and β-hydroxyacyl CoA dehydrogenase activity were measured in 5–10 mg skeletal muscle as previously reported (14).

Electron Microscopy

In the HSP72Tg study, standard processing methods were used. The muscle was fixed in 2.5% glutaraldehyde, osmicated with 2.5% osmium tetroxide, dehydrated through a graded series of acetone solutions, and embedded in epon-araldite. Ultra-thin sections were cut on a Reichert-Jung Ultra-S microtome and collected on Nickel Grids. The sections were stained with uranyl acetate and lead citrate and viewed on a Hitachi H7500 TEM. Random images were taken at a magnification of 20,000. The area of the field of view was calculated, and mitochondria were counted and expressed as number of mitochondria per micrometers squared. Ten different areas of muscle were calculated for each animal and averaged. For the BGP-15 studies, sections were prepared in a similar manner to what is described above; however, they were imaged in a different location on a Hitachi 7100 electron microscope, and mitochondrial areas were calculated by ImageTool (University of Texas Health Science Center, San Antonio, TX).

Seahorse Analyzer

C2C12 myoblasts were transfected with pIRES HSP72 plasmid or empty vector (control) before undergoing selection with geneticin. After 3 weeks of selection, pooled stable myoblasts were seeded to Seahorse V7 plates and induced to differentiate by serum withdrawal. Mitochondrial function of HSP72 overexpressing and control cells was analyzed using the Seahorse XF analyzer as previously described (27).

Muscle Mitochondrial Isolation

Mitochondrial isolation was performed in quadriceps muscle. Fresh tissue (~300 mg) was immediately placed in ice-cold isolation medium (pH 7: 100 mmol/L sucrose, 100 mmol/L KCl, 50 mmol/L Tris-HCl, 1 mmol/L KH_2PO_4, 0.1 mmol/L EGTA, and 0.2% fatty acid–free BSA). After the tissue was chopped in 2 mL fresh ice-cold isolation medium, samples were incubated for 2 min with 1.5 μg proteinase/mg tissue. Samples were homogenized in 6 mL isolation medium with an electric homogenizer. After the samples were spun down for 5 min at 800*g*, the supernatant was centrifuged again at 12,000*g* for 10 min. Mitochondria in the resulting pellet were washed in 1 mL isolation medium and centrifuged at 10,000*g* for 10 min.

Respiratory Measures and AMPK Activity

VO_2 rates (OCR) were measured in isolated mitochondria from the skeletal muscle of WT and HSP72Tg mice fed a normal chow diet using a Clarke Electrode. Basal, ADP-stimulated state III (2.4 mmol/L), state IV, and 2,4-dinitrophenol (DNP)-stimulated uncoupled respiration (0.1 mmol/L) were measured in isolated mitochondria preps in the presence of *1*) complex 1 substrates (5 mmol/L pyruvate, 2 mmol/L malate) and *2*) complex II substrates (10 mmol/L succinate, 4 μmol/L rotenone). OCR was then normalized and expressed relative to citrate synthase activity levels. OCR measurements for isolated mitochondria using the Seahorse Analyzer in Supplementary Fig. 7 were carried out as described in the legend. Total AMPK activity from whole cell lysates was measured as previously described (28).

Fiber Typing

Muscle fiber type was determined in quadriceps muscle by incubation of slides in acidic (pH 4.3) solution containing potassium acetate and $CaCl_2$ $2H_2O$. After 5 min in this solution, slides were then incubated at 37°C in ATP solution followed by room-temperature incubations in 1% $CaCl_2$ 0.2 H_2O, 2% $CoCl_2$ 0.6 H_2O, and 1% ammonium sulphide before being dehydrated in ascending alcohol stocks. Sections were viewed under light microscopy.

Plasma Analysis

Plasma measurements were performed on blood collected from the chest cavity and centrifuged at 14,000*g* for 10

min. Insulin concentrations were measured by ELISA (Linco Research, St. Louis, MO). The concentration of free fatty acids was determined using a colorimetric kit (Wako Pure Chemical Industries, Osaka, Japan). Plasma acylcarnitines were measured as previously described (13).

Statistics

Data were analyzed by two-way ANOVA and Tukey post hoc tests. An unpaired Student *t* test was also used for comparison of relevant groups. All data are presented as mean ± SEM unless otherwise indicated. Statistical significance was set at $P < 0.05$.

RESULTS

HSP72Tg Mice Are Protected From HFD-Induced Obesity and Insulin Resistance

We previously observed that HSP72Tg mice are protected from HFD-induced activation of JNK in vivo (14). To confirm this observation in an acute setting with exposure to higher fatty acid concentrations, we examined whether overexpression of HSP72 could inhibit fatty acid–induced JNK activation in skeletal muscle ex vivo. Consistent with our previous observation, high-dose palmitate treatment resulted in a robust increase in JNK phosphorylation in soleus muscles from WT mice, but this effect was markedly blunted in HSP72Tg mice (Supplementary Fig. 1*A*). Therefore, although it is clear that increasing HSP72 can block JNK activity, whether blockage of proinflammatory signaling is the primary mechanism by which HSP72 protects against HFD-induced insulin resistance is not known. In our previous study (14), mice were fed a diet containing 60% of total energy from fat for 16 weeks, which resulted in an upregulation of JNK phosphorylation in the skeletal muscles from the WT cohort. In the current investigation, we deliberately chose to use a diet containing significantly less lipid (45% of energy from fat) for a shorter time (10 weeks). Contrary to our previous study (14), this dietary intervention did not cause JNK activation in skeletal muscle from either WT or HSP72Tg mice (Supplementary Fig. 1*B*). Nonetheless, this dietary intervention increased body weight (Fig. 1*A*) and fat pad mass (Fig. 1*B*) and induced fasting hyperglycemia (Fig. 1*C*) and hyperinsulinemia (Fig. 1*D*) in WT mice. Importantly, however, these HFD-induced alterations in metabolic homeostasis were prevented in HSP72Tg mice (Fig. 1*A–D*). Consistent with these findings, the HFD promoted glucose intolerance (Fig. 2*A* and *B*) and impaired insulin-stimulated phosphorylation of Akt (Fig. 2*C–E*) in WT mice, whereas the HSP72Tg mice were largely protected from these deleterious effects of the diet. Intriguingly, even on a normal chow diet HSP72Tg mice showed enhanced glucose tolerance (Fig. 2*A*). To assess this finding in more detail, we measured insulin-stimulated glucose clearance into skeletal muscle, white adipose tissue (WAT), and brown adipose tissue in normal chow–fed mice using tracer methodology (for radioactivity and blood glucose graphs during insulin stimulation, see Supplementary Fig. 2*A* and *B*). Insulin-stimulated glucose uptake into the tibialis anterior muscle was increased in HSP72Tg compared with WT mice (Fig. 2*F*), demonstrating that nutrient overload is not necessary for HSP72 overexpression to improve insulin action. We also observed the same increase in insulin-stimulated glucose uptake in both WAT (Fig. 2*G*) and brown adipose tissue (Fig. 2*H*), even though HSP72 was not overexpressed in these peripheral tissues. Interestingly, further analysis of

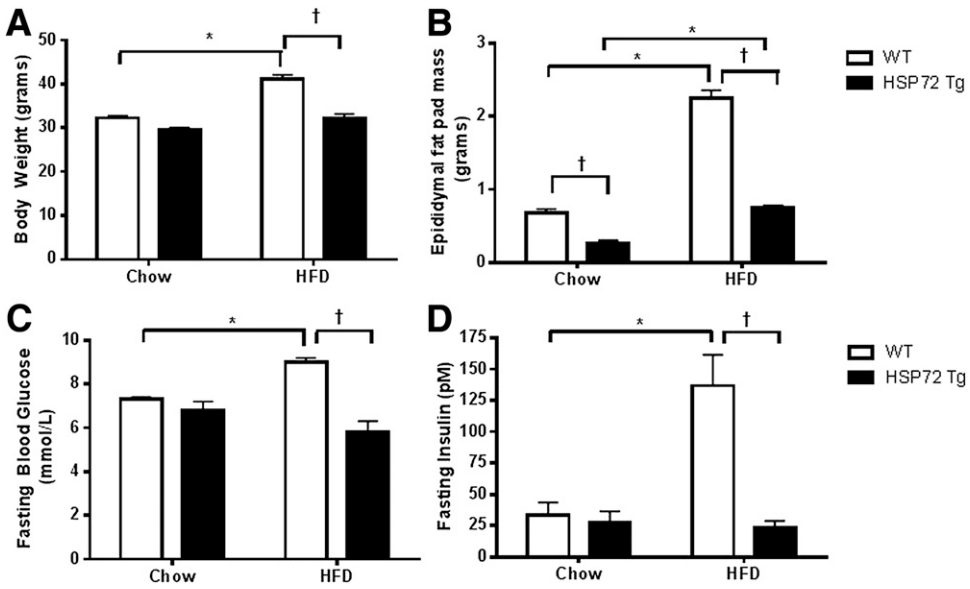

Figure 1—Characteristics of WT and HSP72Tg mice fed a normal chow diet or HFD for 10 weeks. *A*: Body weight. *B*: Epididymal fat pad mass. *C*: Fasting blood glucose. *D*: Fasting insulin. $n = 6–8$. *Diet effect: $P < 0.05$ vs. chow within same genotype. †Genotype effect: $P < 0.05$ vs. WT within same diet.

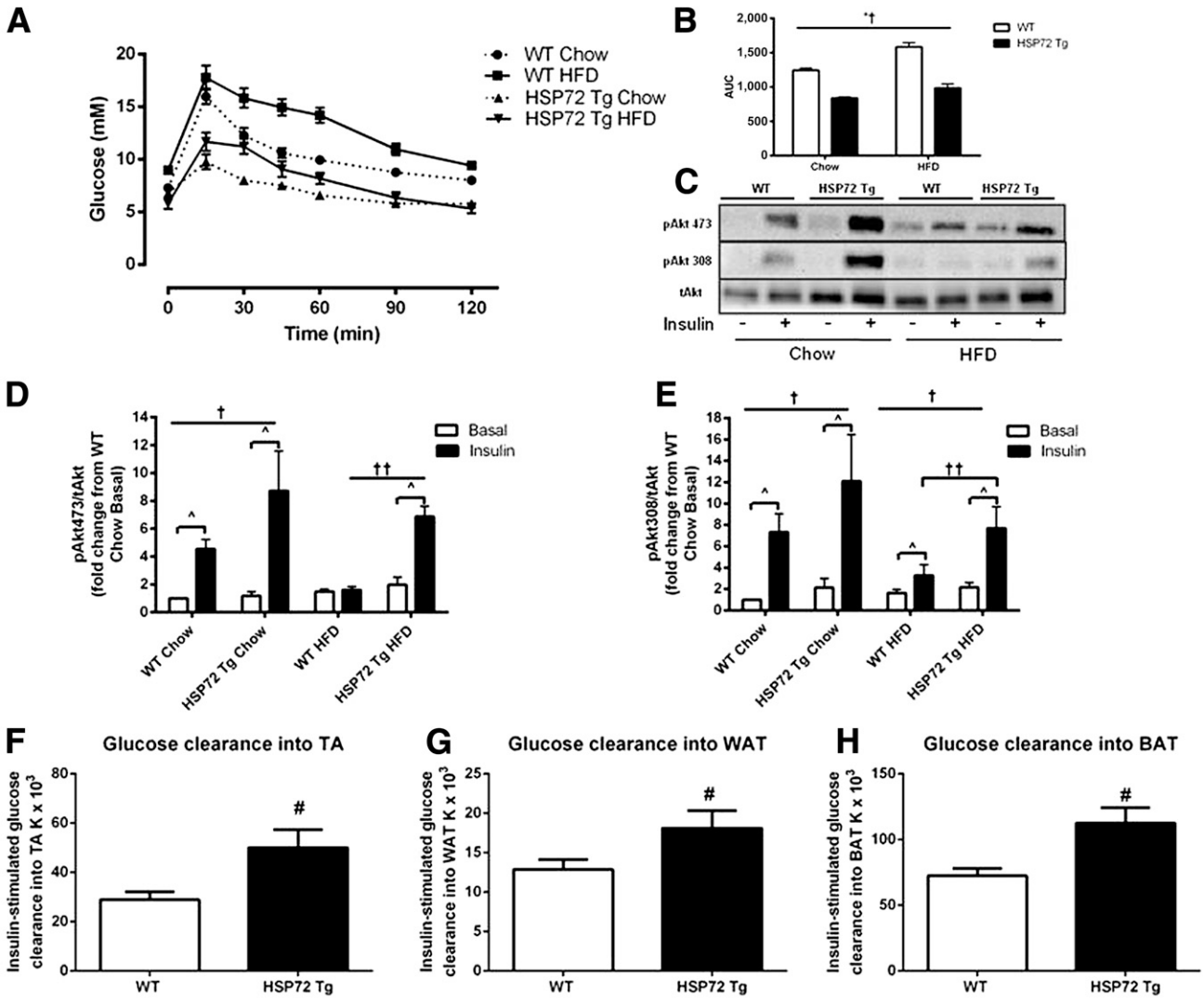

Figure 2—Glucose tolerance test in 5-h fasted WT and HSP72Tg mice fed either a chow diet or HFD for 10 weeks. Blood glucose levels after a glucose injection (1 g/kg i.p.) (*A*) and incremental area under the curve during the glucose tolerance test (*B*) are shown. Insulin-stimulated Akt phosphorylation in WT and HSP72Tg mice fed either a chow diet or HFD for 10 weeks is shown. *C*: Representative immunoblots of phosphorylated and total Akt. Quantification of Akt phosphorylation on Ser^{473} (*D*) and Thr^{308} (*E*), respectively, is shown. n = 6–8 per group. *$P < 0.05$ main effect for diet; †$P < 0.05$ main effect for genotype within diet group; ††genotype effect within treatment (insulin stimulation), $P < 0.05$ vs. WT insulin-stimulated condition; ^treatment effect, $P < 0.05$ basal vs. insulin-stimulated condition within each diet and genotype. *F–H*: Insulin-stimulated glucose clearance into peripheral tissues in chow-fed mice. [^{3}H]2-deoxy-D-glucose clearance into tibialis anterior (TA) skeletal muscle (*F*), WAT from the epididymal fat pad (*G*), and brown adipose tissue (BAT) (*H*) are shown; n = 7–8 per group. #$P < 0.05$ vs. WT. Data are means ± SEM. K × 10^3, the rate of tissue metabolism of [^{3}H]2-deoxy-D-glucose.

the WAT also revealed increased rates of lipolysis and oxidative enzymes citrate synthase and *β-HAD* (Supplementary Fig. 3*A–D*). These initial studies were performed in HSP72Tg and WT mice on a balb/c background. To determine whether the metabolic phenotype observed in these mice was penetrative across different genetic strains of mice, we back-crossed the mice at least 10 generations onto a C57BL/6 background. We showed that under HFD conditions, heterozygous HSP72Tg mice on such a background were leaner and more glucose tolerant compared with littermate control mice (Supplementary Fig. 4*A–F*). Taken together, these findings suggest that HSP72 protects against the development of diet-induced insulin resistance by mechanisms other than blocking JNK activation in skeletal muscle and possibly by indirect action on metabolic tissues that do not express the transgene. In addition, the effect of HSP72 overexpression on metabolic homeostasis is preserved across mice with different genetic backgrounds using littermate mice as controls.

HSP72 Transgenic Mice Exhibit Increased Energy Expenditure, Whole-Body Fat Oxidation, and Skeletal Muscle Fat Oxidation and Are Resistant to HFD-Induced Ectopic Lipid Deposition

HSP72Tg mice were leaner than WT animals (Fig. 1*B*), and this finding could not be explained by food consumption, as energy intake was similar between the genotypes,

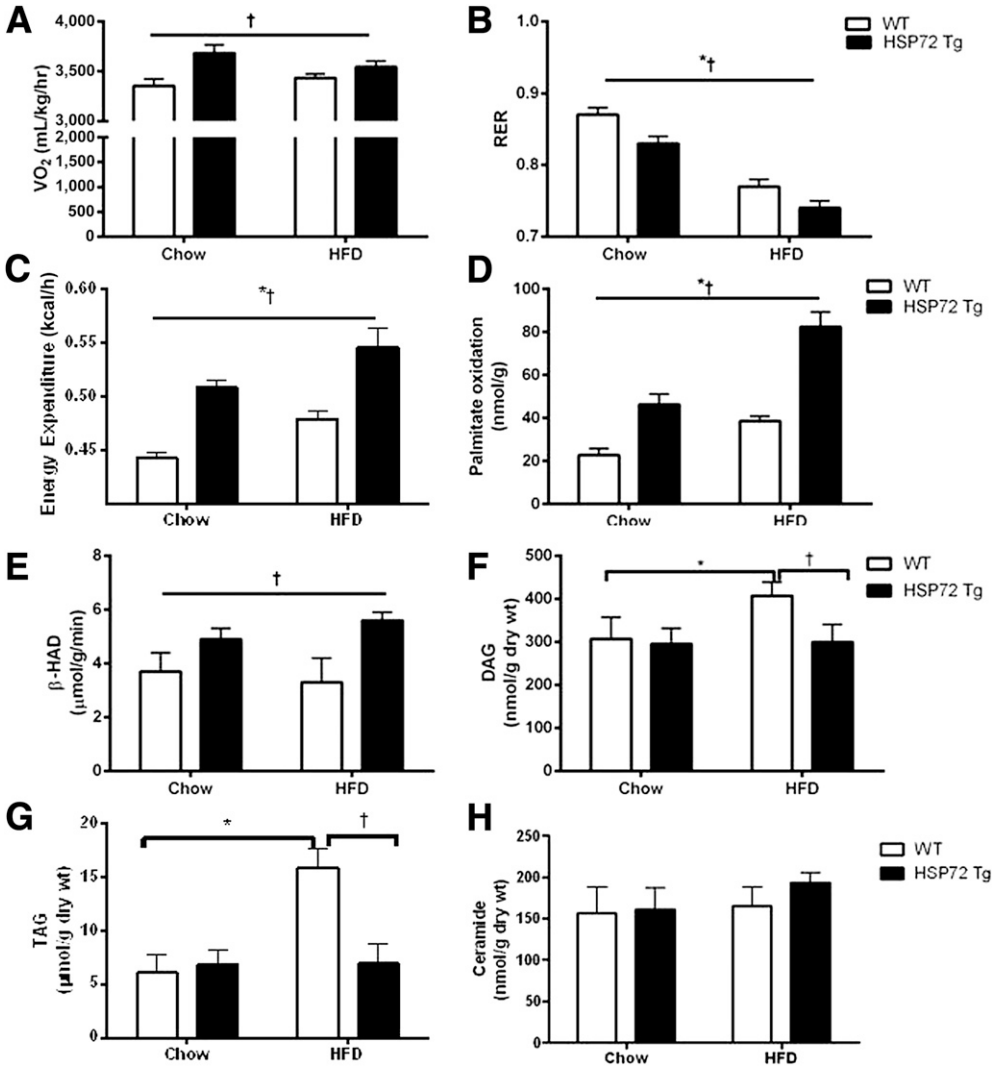

Figure 3—Aspects of whole-body energy metabolism in WT and HSP72Tg mice fed either a chow diet or HFD for 10 weeks. VO_2 (*A*), RER (*B*), and energy expenditure (*C*). Data are means ± SEM; $n = 6$. *$P < 0.05$ main effect for diet, †$P < 0.05$ main effect for genotype. *D–H*: Skeletal muscle lipid levels and palmitate oxidation rates in WT and HSP72Tg mice fed either a chow diet or HFD for 10 weeks. *D*: Palmitate oxidation in isolated soleus muscle. *E*: β-HAD activity in quadriceps muscle. $n = 6$–8 per group. *$P < 0.05$ main effect for diet, †$P < 0.05$ main effect for genotype. *F*: Muscle DAG concentration. *G*: Muscle TAG concentration. *H*: Muscle ceramide concentration. $n = 6$–8 per group. *Diet effect: $P < 0.05$ vs. WT chow; †Genotype effect: $P < 0.05$ vs. high-fat–fed HSP72Tg. Data are means ± SEM. hr, hour.

suggesting that HSP72Tg mice exhibit enhanced energy expenditure compared with WT mice. To examine this further, we measured whole-body VO_2 by indirect calorimetry. HSP72Tg mice exhibited elevated VO_2 compared with WT animals (Fig. 3*A*) with accompanying increase in energy expenditure (Fig. 3*C*). Importantly, this was not due to merely having a lower body weight, since we observed a markedly higher VO_2 in HSP72Tg mice on a chow diet (Fig. 3*A*), when body weight was identical (Fig. 1*A*). In addition, the respiratory exchange ratio (RER) was reduced in HSP72Tg mice, implying that the increased energy expenditure was supported by an increased rate of fat oxidation (Fig. 3*B*). HSP72Tg mice were resistant to HFD-induced weight gain and displayed increased whole-body VO_2 and fat oxidation. As skeletal muscle is an important tissue for lipid metabolism, we next assessed whether skeletal muscle FAO was enhanced in these animals. The HFD increased skeletal muscle FAO irrespective of genotype (Fig. 3*D*) as previously observed (13). Importantly, however, skeletal muscle FAO was markedly elevated in HSP72Tg mice compared with WT animals irrespective of diet (Fig. 3*D*). β-HAD activity was elevated in HSP72Tg mice (Fig. 3*E*), and consistent with increased whole-body fat oxidation (Fig. 3*A*) and skeletal muscle FAO (Fig. 3*D*), we observed a decrease in circulating free fatty acids in HSP72Tg mice compared with WT (normal chow: WT 1.45 ± 0.17 μmol/L, HSP72Tg 0.63 ± 0.13 μmol/L; HFD: WT 1.29 ± 0.15 μmol/L, HSP72Tg 0.88 ± 0.08 μmol/L). Considering that the accumulation of bioactive lipids in skeletal muscle impairs insulin

action, we next examined levels of TAG, DAG, and ceramides in the skeletal muscles from HSP72Tg and WT mice fed a normal chow diet or HFD. The HFD caused an increase in both DAG (Fig. 3*F*) and TAG (Fig. 3*G*) in WT, but this increase was prevented in HSP72Tg mice (Fig. 3*F* and *G*). Ceramide concentrations were neither altered by the HFD nor different between genotypes (Fig. 3*H*). As alterations in PKC isoforms have been linked to lipid-induced alterations in insulin signaling (29), we analyzed three PKC isoforms (θ, α, and δ). While a HFD tended to increase the membrane-to-cytosol ratio in the WT animals, but not in the HSP72Tg mice, there was no significant difference between groups (Supplementary Fig. 5*A–D*). Together, these data suggest that overexpression of HSP72 in skeletal muscle enhances muscle oxidative metabolism, thereby preventing ectopic lipid accumulation in skeletal muscle when animals are challenged with an HFD.

As we had observed reductions in TAG and DAG when HSP72Tg mice were fed an HFD, we next assessed whether HSP72 overexpression affected fatty acid transporters and the lipolytic enzyme machinery of the skeletal muscle. Western blotting analysis revealed a significant increase in the expression of the lipolytic enzyme LPL in the HSP72Tg mice, while no changes were observed for the fatty acid transporter CD36 (Fig. 4*A–C*). We also analyzed the mRNA expression of the genes encoding these two proteins, as well as others involved in fatty acid lipolysis, uptake, and synthesis (Fig. 4*D*). While many of

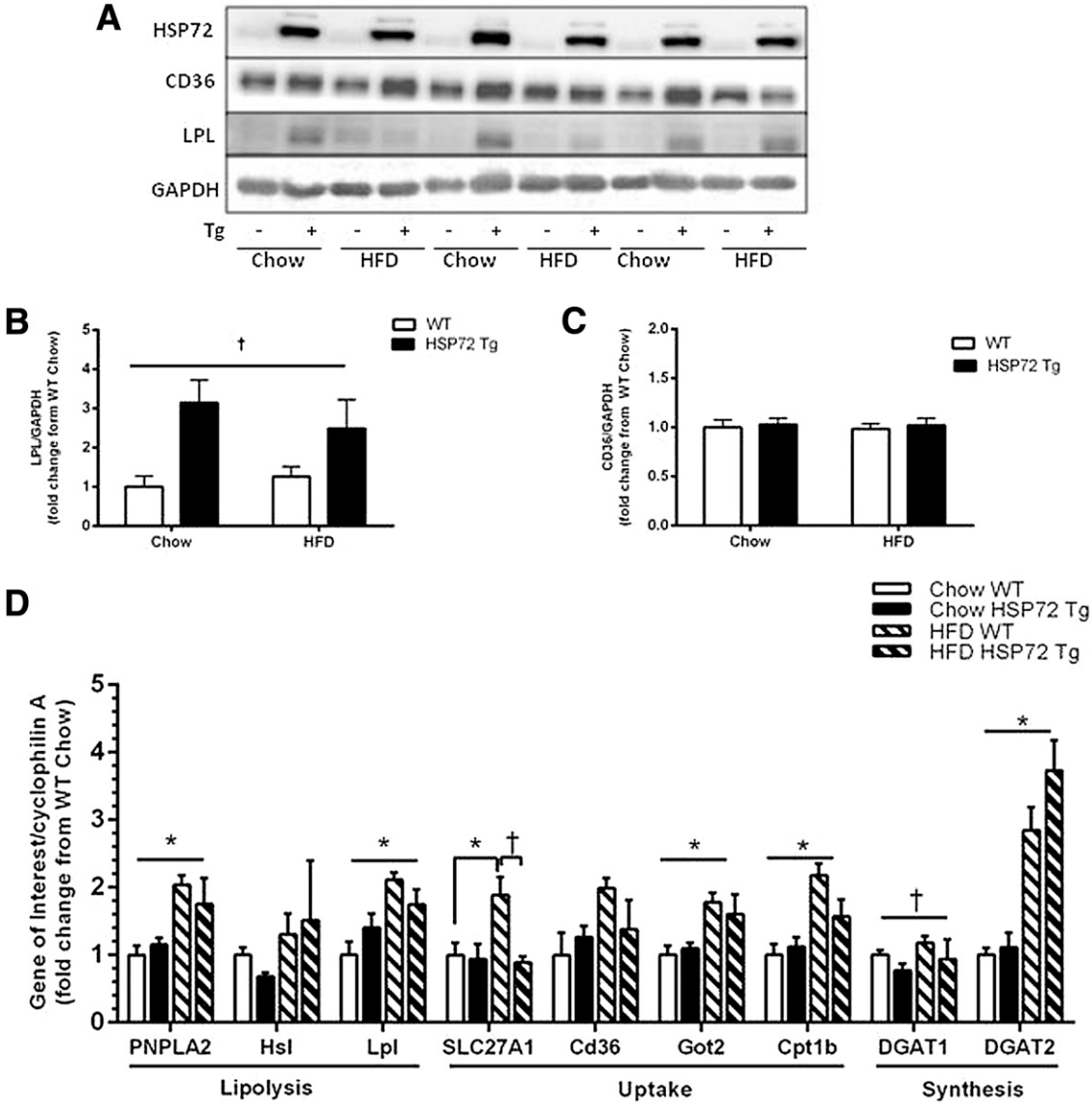

Figure 4—Markers of lipolysis and fatty acid transporters in normal chow– and high-fat–fed mice. *A*: Western blotting analysis for HSP72, CD36, and LPL. Quantification of LPL (*B*) and CD36 protein levels (*C*) relative to glyceraldehyde-3-phosphate dehydrogenase (GAPDH). Data are means ± SEM; $n = 6$. †$P < 0.05$ main effect for genotype. *D*: RT-PCR analysis of various genes related to lipolysis, fatty acid cellular or mitochondrial uptake, and fatty acid synthesis. Data are expressed relative to cyclophilin A levels and are means ± SEM; $n = 4–7$.

these genes were altered with HFD (*PNPLA2*, *LPL*, *SLC27A1*, *Got2*, *CPT1B*, and *DGAT2*), only two were affected by HSP72 overexpression. These were *SLC27A1*, which was significantly decreased in the HSP72Tg mice on an HFD compared with chow, and *DGAT1*, where a main effect was detected for a decrease in expression in the HSP72Tg mice (Fig. 4*D*). As the *LPL* mRNA was not different between genotypes, it is likely that the overexpression of HSP72 increased LPL protein expression posttranslationally in a chaperone-dependent manner.

HSP72Tg Mice Have Increased Number of Mitochondria and Superior Running Performance

To determine the gene expression signature that underlies the enhanced metabolic phenotype observed in the HSP72Tg mice, we next performed microarray analyses on skeletal muscle from both genotypes of mice. We used Gene Set Enrichment Analyses, previously described (21), but no differences were observed for genes associated with the tricarboxylic acid cycle, electron transport chain, or oxidative phosphorylation (data not shown) when comparing the cohorts. Slow oxidative muscle fiber content was also not different in the quadriceps muscle between HSP72Tg and WT mice (Supplementary Fig. 6*A*). Next, we investigated the functional capacity of mitochondria from quadriceps muscle of the HSP72Tg and WT mice by measuring relative VO_2 rates in response to ADP and the chemical uncoupler (DNP). We observed no difference in OCR, per unit of mitochondria, between the HSP72Tg mice and WT in the basal state, in response to ADP or DNP (Supplementary Fig. 6*B* and *C*) or in the HSP72Tg backcrossed mice on a normal chow diet or HFD (Supplementary Fig. 7*A*–*D*). As there was no difference in muscle fiber type or mitochondrial respiratory capacity (per unit mitochondria), we next tested whether muscles from HSP72Tg mice contain a greater number of mitochondria. Recent work suggests that heat stress–induced HSP72 expression stimulates mitochondrial biogenesis (18). Accordingly, we performed electron microscopy studies to quantify the number of mitochondria in the quadriceps muscles of the HSP72Tg and WT mice. We observed an ~50% increase in the number of mitochondria in the HSP72Tg relative to WT mice (Fig. 5*A*). Thus, although functional capacity per unit mitochondria was not different between the genotypes, HSP72 overexpression in

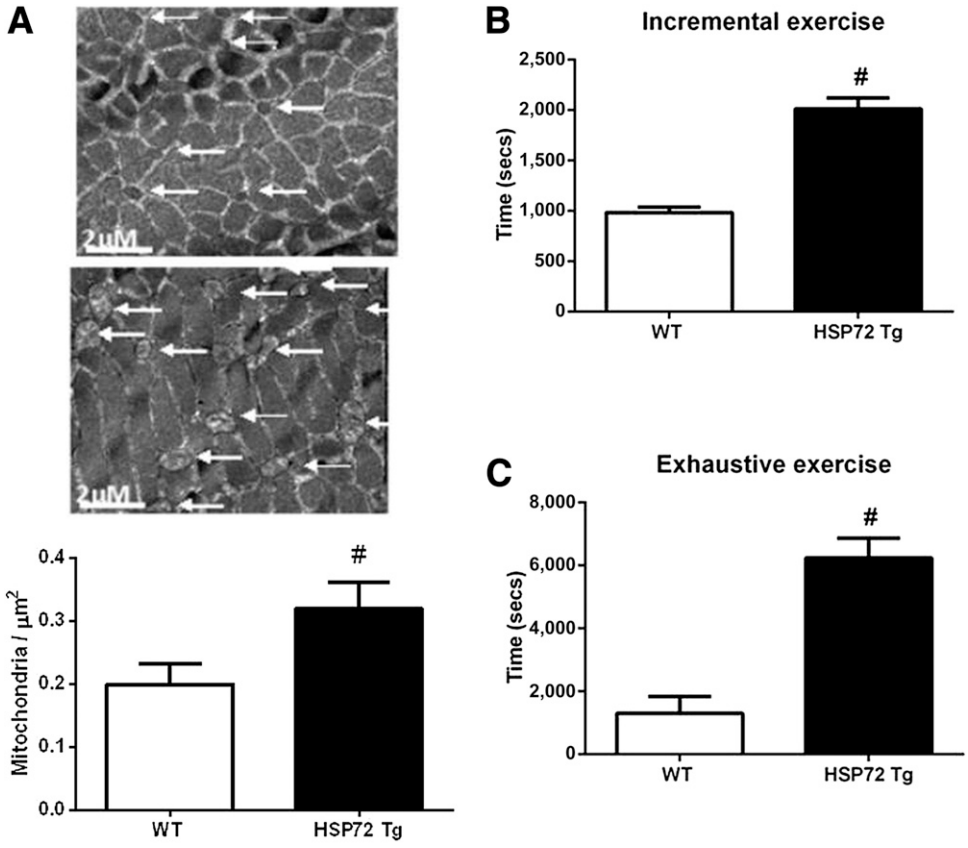

Figure 5—Mitochondrial number via electron microscopy imaging in WT and HSP72Tg mice fed a chow diet. *A*: Representative pictures and quantification from quadriceps muscle sections from WT and HSP72Tg mice. The arrows indicate mitochondria; $n = 10–11$. #$P \leq 0.05$ WT vs. HSP72Tg. *B* and *C*: Endurance running capacity in chow-fed WT and HSP72Tg mice. *B*: Running time during an incremental running test to fatigue. *C*: Time to fatigue during a treadmill run at fixed speed and gradient. $n = 5–10$ per group. #$P < 0.05$ vs. WT. Data are means ± SEM. secs, seconds.

muscle increased the abundance of mitochondria in that tissue. Increased mitochondrial density does not necessarily equate to increased mitochondrial function. Since increased functional mitochondrial number and muscle oxidative metabolism are usually associated with increased exercise endurance, we next examined running performance. Treadmill running including both an incremental exercise test (Fig. 5*B*) and time to voluntary exhaustion (Fig. 5*C*) was assessed. Irrespective of the test type, HSP72Tg mice exhibited a markedly enhanced exercise capacity (Fig. 5*B* and *C*). Interestingly, while impaired mitochondrial capacity is associated with the pathogenesis of insulin resistance and type 2 diabetes (8,9), others have suggested that increasing energetic flux through the mitochondria may result in incomplete β-oxidation and alterations in plasma acylcarnitines, which may lead to insulin resistance (30). Accordingly, we next measured plasma acylcarnitines in our model. Consistent with a previous study (30), we observed that some acylcarnitine species increased, while others decreased when mice were placed on an HFD (Supplementary Fig. 8) In addition, the total plasma acylcarnitine levels are slightly, but significantly, reduced on HFD. However, despite the marked effect of HSP72 overexpression on mitochondrial energy turnover as measured by several methods, the plasma acylcarnitine levels comparing WT and HSP72Tg animals were very similar, irrespective of diet (Supplementary Fig. 8), providing solid evidence that muscle oxidative capacity is uncoupled from plasma acylcarnitine levels, at least in our model. Together, these data indicate that elevated HSP72 expression drives an increase in mitochondrial number and oxidative metabolism and enhances exercise performance and insulin action in mice.

HSP72Tg Mice Display Upregulation of Tfam Transcription, Enhanced AMPK Activity, and Increased SIRT1 Protein Expression

Considering that muscle from HSP72Tg mice displayed an increased mitochondria number and enhanced oxidative metabolism, we next examined known regulators of these pathways. The PGC-1 family of transcriptional coactivators, putative regulators of mitochondrial oxidative metabolism (31,32), target the transcription factor Nrf-1 to stimulate the expression of Tfam, a matrix protein essential for the replication and transcription of mitochondrial DNA (31). Although skeletal muscle PGC-1α mRNA was not different when comparing HSP72Tg with WT, Tfam mRNA was twofold higher in HSP72Tg (Fig. 6*A*). PGC-1α is directly linked to the activity of AMPK (33), an evolutionarily conserved sensor of cellular energy status, critical for enhancing fuel metabolism (34). Indeed, AMPK phosphorylation (Thr^{172}) (Fig. 6*B*) and activity (Fig. 6*C*) was enhanced in the muscles from HSP72Tg relative to WT mice. Another important fuel-sensing molecule is the NAD^+-dependent deacetylase SIRT1, an important regulator of oxidative metabolism (12,35). AMPK and SIRT1 regulate each other and share many common target molecules (36). Accordingly, we examined whether SIRT1 expression and activation were affected by HSP72 overexpression. While SIRT1 mRNA expression tended (NS, $P = 0.1$) to be increased in HSP72Tg mice (Fig. 6*A*), SIRT1 protein levels were higher in the HSP72Tg relative to WT mice irrespective of diet (Fig. 6*D*). Given that SIRT1 is known to deacetylate PGC-1α (37), we performed immunoprecipitation experiments to investigate PGC-1α acetylation levels, but we failed to detect differences between HSP72Tg and WT mice (Supplementary Fig. 9*A*), and we did not we see any difference between the groups in total PGC-1α expression from whole tissue lysates (Supplementary Fig. 9*B*).

As PGC-1α was not altered, it was possible that HSP72Tg overexpression could reduce the degradation of mitochondria. To address this question, we next investigated any changes in autophagy/mitophagy in the skeletal muscle of the HSP72Tg mice. As shown in Supplementary Fig. 10*A–F*, we observed a general increase in autophagy in the skeletal muscle of the HSP72Tg mice fed an HFD. Both p62, a ubiquitin-binding scaffold protein that is degraded with autophagy, and ATG12, a part of a complex involved in the recruitment of LC3A levels, were reduced in HSP72Tg animals fed an HFD (Supplementary Fig. 10). In addition, LC3A, a marker for the autophagasome membrane, tended to be increased in the HSP72Tg mice (Supplementary Fig. 10). To further examine the relationship between HSP72 overexpression and autophagy, we next collected skeletal muscle from animals that had been killed either in the fed state or after a 24-h fast. Fasting increased the level of LC3A conversion and decreased ATG12 protein expression, while p62 was unchanged (Supplementary Fig. 10*G–K*). Interestingly, the HSP72Tg mice displayed greater LC3A conversion in the fasted state and less ATG12 expression (Supplementary Fig. 10*G–K*), again indicating increased autophagy and greater turnover of organelles in the skeletal muscle. To determine whether we could detect any specific differences in mitophagy markers (the mitochondrial specific autophagic degradation process), we blotted for the E3 ubiquitin ligase parkin and the PTEN-induced putative kinase 1 (PINK1). No significant differences were observed between HSP72Tg and WT mice for these proteins (Supplementary Fig. 11*A–C*); however a significantly greater quantity of p53 (a tumor suppressor protein linked to both increased and decreased autophagy) was observed in the HSP72Tg muscle (Supplementary Fig. 11*D* and *E*). Of note, p53 has recently been shown to inhibit parkin-mediated mitophagy (38). Finally, we looked at mitochondrial fusion and fission factors (Supplementary Fig. 11*F–J*). Mitochondrial morphology is a highly dynamic process regulated by the balance of fission and fusion processes (39). These processes also impact on mitophagy and, therefore, impact on mitochondrial quantity. Mitochondrial outer membrane proteins mitochondrial fission factor (MFF) and mitochondrial fission protein 1 (Fis1) are thought to regulate mitochondrial fission via recruitment of dynamin-related protein 1 (DRP1) to the mitochondria. Interestingly MFF was decreased in the HSP72Tg mice, whereas Fis1 was increased (Supplementary Fig. 11*F*, *H*,

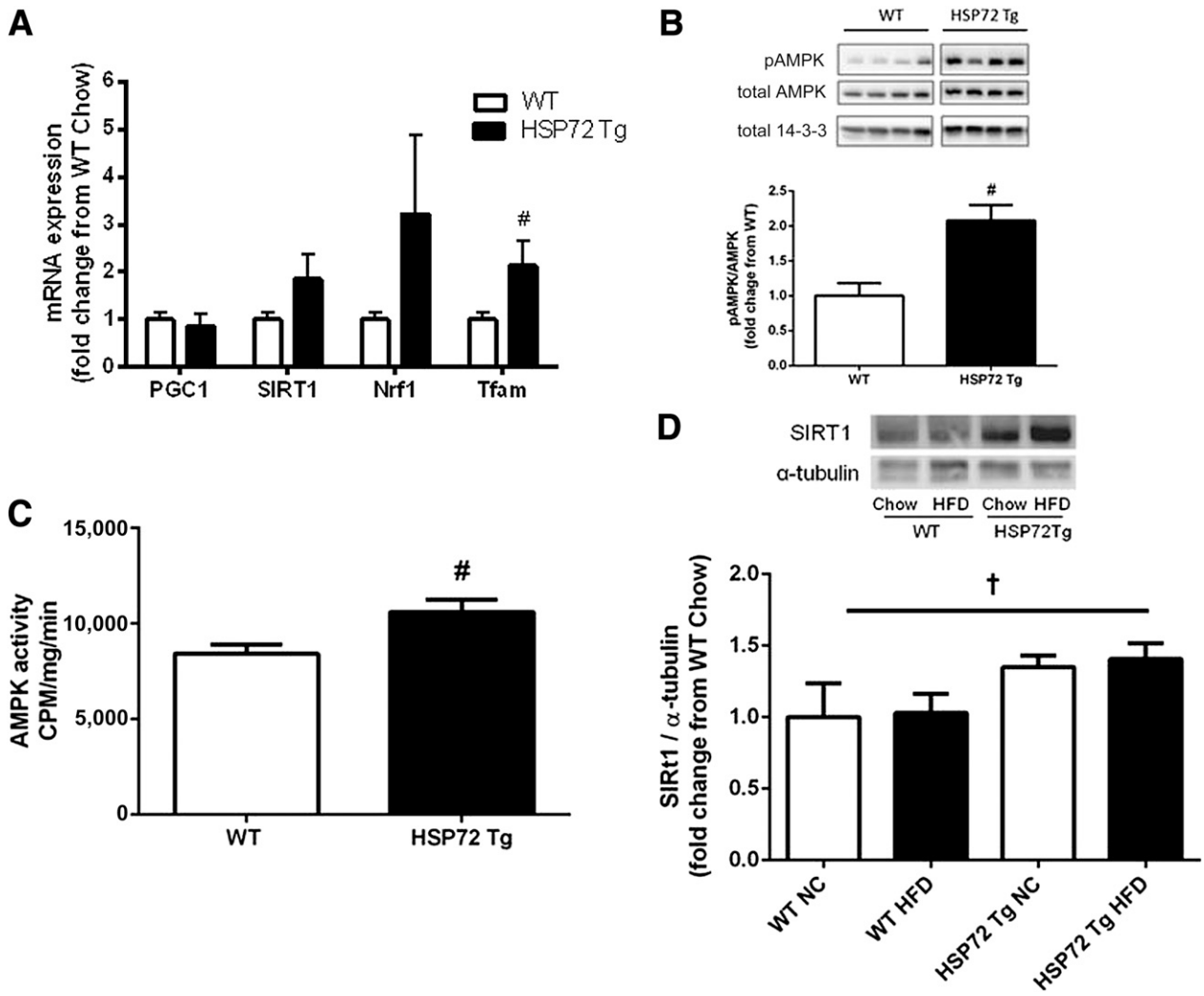

Figure 6—RT-PCR analysis of skeletal muscle and AMPK phosphorylation and activity. *A*: Genes related to mitochondrial biogenesis in skeletal muscle (Pgc-1α, SIRT1, nuclear respiratory factor 1, and Tfam) in WT and HSP72Tg mice fed a normal chow diet; $n = 6$. #$P < 0.05$ WT vs. HSP72Tg. *B*: Representative blot and quantification of phosphorylation of AMPK (Thr^{172}). *C*: AMPK activity levels form skeletal muscle lysates. $n = 4$ per group for phosphorylation, $n = 14$ per group for activity. #$P < 0.05$ WT vs. HSP72Tg. *D*: SIRT1 protein expression in skeletal muscle from WT and HSP72Tg mice fed either a chow diet or HFD for 10 weeks. *D*: Representative immunoblot and quantification of SIRT1 expression; $n = 6$ per group. †$P < 0.05$ main effect for genotype. NC, normal chow.

and *J*), theoretically opposing each other's actions. Optic atrophy 1 (Opa1), a protein linked to mitochondrial fusion and the phosphorylation of DRP-1 at Ser^{637}, was not different between groups (Supplementary Fig. 11*F*, *G*, and *I*). Together, these data indicate that while autophagy may be elevated in the HSP72Tg muscle, mitophagy, fission, and/or fusion processes do not appear to be markedly affected by HSP72 overexpression, although further research is required to clarify the role of HSP72 in these mitochondrial dynamic processes.

Overexpression of HSP72 Increases Cellular Respiration, While the HSP72 Coinducer BGP-15 Increases Mitochondrial Number in a Diabetic Rodent Model

In order to determine whether the increase in mitochondrial number observed in the HSP72Tg mice was preserved across different experimental models and in an environment free of the confounding effects of any circulating factor/s, we next measured OCR in skeletal myotubes engineered to stably overexpress HSP72 (Fig. 7*A*). These cells displayed significantly increased basal and maximal respiration rates compared with control cells (Fig. 7*B*). Importantly, supportive of the interpretation that a mitochondrial phenotype drives the increase in energy expenditure and protection from diet-induced obesity and insulin resistance, the increase in basal respiration was due to increased ATP turnover rate (Fig. 7*B*). Furthermore, there was a trend for an increase in glycolysis (extracellular acidification rate is a proxy measure of glycolysis) in the cells stably expressed with HSP72 (Supplementary Fig. 12*A* and *B*), indicating an overall increase in cellular bioenergetics and substrate oxidation in the cells stably overexpressing HSP72.

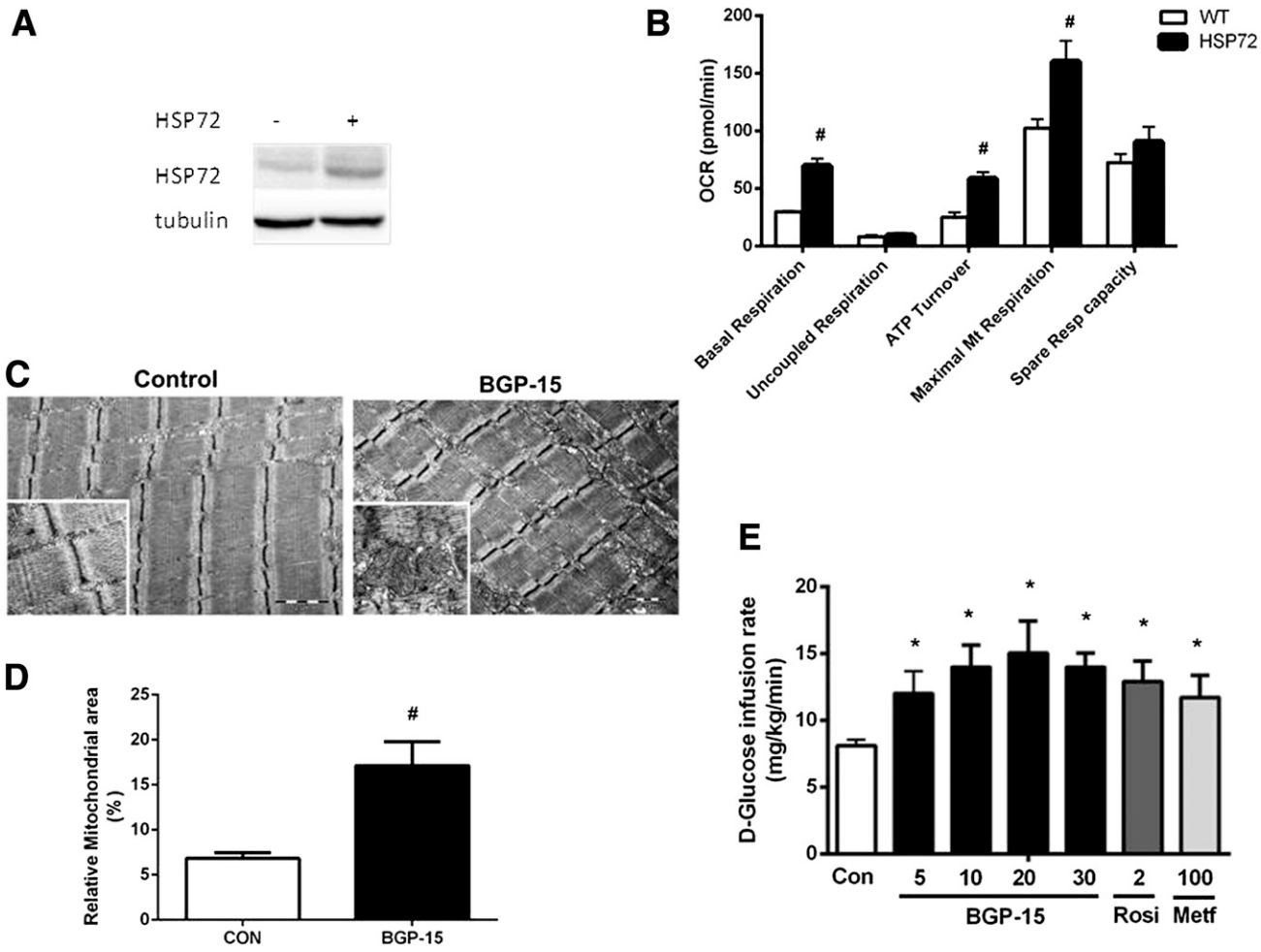

Figure 7—VO_2 analysis in HSP72 stably expressed myotube cell line. *A*: Western blot of HSP72 stably overexpressed cells and WT cells. *B*: Analysis from mitochondrial function test for basal respiration, uncoupled respiration, ATP turnover, maximal mitochondrial (Mt) respiration, and spare respiratory (Resp) capacity. Addition of compounds at the straight lines was as follows: oligomycin, trifluorocarbonylcyanide phenylhydrazone (FCCP), and antimycin A. #$P < 0.05$ relative to control group. *C* and *D*: BGP-15 treatment of the GK rat for five days at 20 mg/kg increases mitochondria number. Representative electron micrographs (*C*) and quantification of BGP-15–stimulated mitochondrial biogenesis (*D*). #$P < 0.05$ relative to control (CON) group, $n = 36$ for BGP-15 treatment and $n = 41$ for control group. *E*: Glucose infusion rate as measured by hyperinsulinemic-euglycemic clamp after BGP-15 treatment. GK rats were administered daily oral doses of BGP-15 (5, 10, 20, and 30 mg/kg), rosiglitazone (Rosi) (2 mg/kg), metformin (Metf) (100 mg/kg), or vehicle for five days. Insulin sensitivity was evaluated after 5 days using the hyperinsulinemic-euglycemic clamp method. Data expressed as mean ± SEM, $n = 6$ animals per group. *$P < 0.05$ relative to control (Con) group.

We have previously demonstrated that the HSP72 coinducer BGP-15 increases HSP72 expression in skeletal muscle (14). Moreover, BGP15 treatment improved insulin sensitivity in *ob/ob* mice (14) and patients with type 2 diabetes (20). Given our findings thus far, we next examined the effect of BGP-15 treatment on mitochondrial density in skeletal muscles from GK rats, a nonobese Wistar substrain that develops type 2 diabetes early in life (40). BGP-15 treatment increased the relative mitochondrial area (Fig. 7*C*) in skeletal muscle of rats compared with vehicle treated. In addition, consistent with our previous observations in both mice (14) and humans (20), BGP-15 was equally as effective as either metformin or rosiglitazone in improving insulin action in GK rats (Fig. 7*D*) Together, these data suggest that the increasing HSP72 expression in vivo by transgenesis, in cells stably transfected to overexpress HSP72 or via pharmacological activation of HSP72 in vivo, increases mitochondrial number, function, and capacity.

DISCUSSION

It is clear that the induction of HSP72 in skeletal muscle can protect mice from HFD-induced insulin resistance. However, the mechanism by which this occurs has remained unclear, since HSP72 can block JNK signaling in skeletal muscle and increase oxidative metabolism, both of which can protect against insulin resistance (14). Herein, we provide new evidence showing that increased skeletal muscle HSP72 expression elevated whole-body energy utilization and FAO, thereby preventing intramuscular

lipid accumulation and insulin resistance independent of changes in proinflammatory signaling. Moreover, increased muscle HSP72 promotes mitochondrial biogenesis and enhanced oxidative metabolism, likely via a mechanism involving increased AMPK activity and sirtuin activation.

In the current investigation, whole-body VO_2, skeletal muscle FAO, and running capacity were increased in HSP72Tg mice compared with WT controls. Consistent with an enhanced oxidative metabolism phenotype, HSP72Tg mice exhibited a reduced RER reflective of a greater reliance on FAO, and this functional readout is consistent with the observed increases in Tfam mRNA expression, AMPK activity, SIRT1 expression, and, indeed, mitochondrial number. Even though our data suggest that mitochondrial biogenesis (i.e., synthesis) is responsible for the increased mitochondrial number observed in the HSP72Tg mice or in mice treated with BGP-15, we cannot dismiss the potential for HSP72 to improve the maintenance of mitochondrial quality and potential slowing of organelle turnover. Indeed, we show that markers of autophagy were increased in HSP72Tg mice (Supplementary Fig. 10). HSP72 is well known to function as a chaperone-mediated stabilizer of a number of enzymes and/or nuclear receptors and aids in the delivery of nuclear encoded proteins to the mitochondrial membrane for mitochondrial importation (41). We therefore cannot rule out chaperone-mediated mitochondrial stabilization as a factor contributing to the observed phenotype.

Despite the fact that we observed an increase in Tfam expression and mitochondria number, we failed to detect any increases in mRNA, protein expression, or acetylated lysine levels of PGC-1α in our study. This was most unexpected given the known role of PGC-1α in regulating mitochondria biogenesis. While unlikely, it is possible that HSP72 somehow regulates Tfam expression in a yet-to-be determined manner independently of PGC-1α. In support of this notion, exercise training in PGC-1α–deficient mice induced expression of genes involved in oxidative phosphorylation, demonstrating that PGC-1α is not mandatory for at least some alterations in oxidative metabolism after endurance training (42,43).

Interestingly, despite HFD-induced increases in TAG and DAG in skeletal muscle, ceramide levels were not elevated, suggesting that increased ceramide accumulation in skeletal muscle is not necessary to induce insulin resistance, as previously demonstrated (3). Of interest, LPL protein expression was increased in skeletal muscle of the HSP72Tg relative to WT mice (Fig. 4*A* and *B*). LPL functions to hydrolyze serum triglycerides releasing fatty acids, which can be internalized into the myocyte. It was recently demonstrated that decreased mitochondrial content in muscle of insulin-resistant offspring may be due, in part, to reductions in LPL expression (44). Hence, it is possible that the effect of HSP72 overexpression on LPL protein expression could explain, in part, the improvement in insulin action in the HSP72Tg mice.

Despite these extensive data suggesting that mitochondria play a role in insulin resistance, they are nonetheless associative, and it has been argued that there is no causal link between mitochondrial dysfunction and insulin resistance (45). Although they are relatively understudied and often overlooked, there are studies from patients with mitochondrial myopathies that support the contention that impaired mitochondrial function and insulin resistance are causally linked. A genetic point mutation affecting position 3243 in the tRNA leucine mitochondrial gene results in poor insulin sensitivity in these patients (46) and maternally transmitted type 2 diabetes (47). In addition, patients with one of the most common mitochondrial diseases, chronic progressive external ophthalmoplegia, have impaired glucose tolerance (48). Taken together, our current data and these previous studies argue that the mitochondria may be a potential target organelle for the treatment of skeletal muscle insulin resistance and type 2 diabetes. Importantly BGP-15, which activates HSP72 and results in increased mitochondria and insulin action (Fig. 7*C* and *D*), is currently the subject of a multicenter human clinical trial for the treatment of type 2 diabetes.

While our study focused on HFD-induced insulin resistance, our observations may have broader consequences for several conditions where mitochondrial function is compromised. It has been suggested that mitochondrial dysfunction (e.g., reduced mitochondrial quality, excessive production of radical oxygen species, and increased mitochondrial DNA mutation rate) plays a critical role in the aging process (49). Indeed, lower respiratory capacity is a characteristic feature of aged human skeletal muscle (50–52). Of note, in a mouse model that phenocopies premature human aging (the PolyG mouse), endurance exercise rescued the accelerating aging phenotype in this model by improving mitochondrial number and function (53). Although not a classical mitochondrial disorder, Duchenne muscular dystrophy is also a condition associated with mitochondrial dysfunction (54,55). Importantly, we recently demonstrated that increasing intramuscular HSP72 expression preserves muscle strength and ameliorates the dystrophic pathology in two mouse models of muscular dystrophy (56). Moreover, when we treated a mouse model that phenocopies Duchenne muscular dystrophy, with BGP-15 both muscle function and life span were increased (56). Given the results presented herein, it would be interesting to determine whether mitochondrial dynamics were altered in the dystrophic models with HSP72 overexpression or BGP-15 treatment. Unfortunately, despite the well-known benefits of exercise, patients suffering these diseases either cannot (e.g., morbidly obese individuals or boys with severe muscular dystrophy) or will not exercise. Exercise training, therefore, has limited long-term efficacy as a primary and sole strategy in treating these conditions. Importantly, our current data provide a realistic therapeutic avenue for treatment.

In summary, we demonstrate that skeletal muscle–specific overexpression of HSP72 protects against obesity-induced insulin resistance via upregulation of oxidative metabolism. This heightened oxidative metabolism and reduced accumulation of deleterious lipid species after high-fat feeding likely promotes insulin sensitivity and glucose tolerance in high-fat–fed HSP72Tg mice. Importantly, in terms of therapeutic potential, the small molecule HSP72 coinducing compound BGP-15 mimics much of the beneficial effect of genetic overexpression of HSP72 and exercise training including increased mitochondria area and insulin sensitivity, suggesting that BGP-15 may offer therapeutic utility in the treatment of diseases associated with metabolic and mitochondrial dysfunction.

Acknowledgments. The authors acknowledge Deb Ramsay and her team at the Alfred Medical Research and Education Precinct Animal Services for their assistance with the animal studies. The authors also acknowledge George Muscat and Natalie Eriksson from the University of Queensland for their helpful discussions and technical assistance. This manuscript is dedicated to Nadine Watson, who passed away during the preparation of the manuscript.

Funding. This study was supported by grants from the National Health and Medical Research Council of Australia (National Health and Medical Research Council [NHMRC] Project grant 1004441 to M.A.F., C.R.B., M.H., and S.L.M.) and the Victorian Government Operational Infrastructure Support Program. C.R.B. and S.L.M. are supported by Career Development Awards of the NHMRC. B.G.D. is supported by an Overseas Postdoctoral Fellowship of the NHMRC and a University of California, Los Angeles (UCLA), Jonsson Cancer Centre Foundation Fellowship. M.J.W. is a Senior Research Fellow and M.A.F. a Senior Principal Research Fellow of the NHMRC. D.C.H. is supported by a National Heart Foundation Biomedical Postdoctoral Fellowship and an Australian Diabetes Society Skip Martin Fellowship. R.S.L.-Y. is supported by NHMRC Project grant 1004212. A.L.H. is supported by the UCLA Department of Medicine and the National Institutes of Health (R01DK78760, R01DK089109, and P30DK063491).

Duality of Interest. M.A.F. is Chief Scientific Officer and K.T. and A.K. are employees of N-Gene Research Laboratories, Inc. No other potential conflicts of interest relevant to this article were reported.

Author Contributions. D.C.H. and C.R.B. designed research, performed and/or analyzed research, wrote the manuscript, and contributed to writing the final submitted version. B.G.D., K.T., A.K., E.E., J.C., N.W., T.G., R.S.L.-Y., T.C., M.J.W., K.C., M.H., and S.L.M. performed and/or analyzed research and contributed to writing the final submitted version. A.L.H. performed and/or analyzed research, wrote the manuscript, and contributed to writing the final submitted version. M.A.F. designed research, wrote the manuscript, and contributed to writing the final submitted version. D.C.H. and K.T. are the guarantors of this work and, as such, had full access to all the data in the study and take responsibility for the integrity of the data and the accuracy of the data analysis.

References

1. Savage DB, Petersen KF, Shulman GI. Disordered lipid metabolism and the pathogenesis of insulin resistance. Physiol Rev 2007;87:507–520

2. Chibalin AV, Leng Y, Vieira E, et al. Downregulation of diacylglycerol kinase delta contributes to hyperglycemia-induced insulin resistance. Cell 2008;132:375–386

3. Yu C, Chen Y, Cline GW, et al. Mechanism by which fatty acids inhibit insulin activation of insulin receptor substrate-1 (IRS-1)-associated phosphatidylinositol 3-kinase activity in muscle. J Biol Chem 2002;277:50230–50236

4. Holland WL, Brozinick JT, Wang LP, et al. Inhibition of ceramide synthesis ameliorates glucocorticoid-, saturated-fat-, and obesity-induced insulin resistance. Cell Metab 2007;5:167–179

5. Morino K, Petersen KF, Shulman GI. Molecular mechanisms of insulin resistance in humans and their potential links with mitochondrial dysfunction. Diabetes 2006;55(Suppl 2):S9–S15

6. Mootha VK, Lindgren CM, Eriksson KF, et al. PGC-1alpha-responsive genes involved in oxidative phosphorylation are coordinately downregulated in human diabetes. Nat Genet 2003;34:267–273

7. Patti ME, Butte AJ, Crunkhorn S, et al. Coordinated reduction of genes of oxidative metabolism in humans with insulin resistance and diabetes: Potential role of PGC1 and NRF1. Proc Natl Acad Sci U S A 2003;100:8466–8471

8. Petersen KF, Befroy D, Dufour S, et al. Mitochondrial dysfunction in the elderly: possible role in insulin resistance. Science 2003;300:1140–1142

9. Petersen KF, Dufour S, Befroy D, Garcia R, Shulman GI. Impaired mitochondrial activity in the insulin-resistant offspring of patients with type 2 diabetes. N Engl J Med 2004;350:664–671

10. Merrill GF, Kurth EJ, Hardie DG, Winder WW. AICA riboside increases AMP-activated protein kinase, fatty acid oxidation, and glucose uptake in rat muscle. Am J Physiol 1997;273:E1107–E1112

11. Narkar VA, Downes M, Yu RT, et al. AMPK and PPARdelta agonists are exercise mimetics. Cell 2008;134:405–415

12. Milne JC, Lambert PD, Schenk S, et al. Small molecule activators of SIRT1 as therapeutics for the treatment of type 2 diabetes. Nature 2007;450:712–716

13. Bruce CR, Hoy AJ, Turner N, et al. Overexpression of carnitine palmitoyltransferase-1 in skeletal muscle is sufficient to enhance fatty acid oxidation and improve high-fat diet-induced insulin resistance. Diabetes 2009;58:550–558

14. Chung J, Nguyen AK, Henstridge DC, et al. HSP72 protects against obesity-induced insulin resistance. Proc Natl Acad Sci U S A 2008;105:1739–1744

15. Gupte AA, Bomhoff GL, Swerdlow RH, Geiger PC. Heat treatment improves glucose tolerance and prevents skeletal muscle insulin resistance in rats fed a high-fat diet. Diabetes 2009;58:567–578

16. Morino S, Kondo T, Sasaki K, et al. Mild electrical stimulation with heat shock ameliorates insulin resistance via enhanced insulin signaling. PLoS One 2008;3:e4068

17. Hirosumi J, Tuncman G, Chang L, et al. A central role for JNK in obesity and insulin resistance. Nature 2002;420:333–336

18. Liu CT, Brooks GA. Mild heat stress induces mitochondrial biogenesis in C2C12 myotubes. J Appl Physiol (1985) 2012;112:354–361

19. Bruce CR, Carey AL, Hawley JA, Febbraio MA. Intramuscular heat shock protein 72 and heme oxygenase-1 mRNA are reduced in patients with type 2 diabetes: evidence that insulin resistance is associated with a disturbed antioxidant defense mechanism. Diabetes 2003;52:2338–2345

20. Literáti-Nagy B, Kulcsár E, Literáti-Nagy Z, et al. Improvement of insulin sensitivity by a novel drug, BGP-15, in insulin-resistant patients: a proof of concept randomized double-blind clinical trial. Horm Metab Res 2009;41:374–380

21. Matthews VB, Allen TL, Risis S, et al. Interleukin-6-deficient mice develop hepatic inflammation and systemic insulin resistance. Diabetologia 2010;53:2431–2441

22. Cooney GJ, Astbury LD, Williams PF, Caterson ID. Insulin response in individual tissues of control and gold thioglucose-obese mice in vivo with [1-14C]2-deoxyglucose. Diabetes 1987;36:152–158

23. Hom FG, Goodner CJ, Berrie MA. A [^{3}H]2-deoxyglucose method for comparing rates of glucose metabolism and insulin responses among rat tissues in vivo. Validation of the model and the absence of an insulin effect on brain. Diabetes 1984;33:141–152

24. Bruce CR, Risis S, Babb JR, et al. The sphingosine-1-phosphate analog FTY720 reduces muscle ceramide content and improves glucose tolerance in high fat-fed male mice. Endocrinology 2013;154:65–76

25. Bruce CR, Dyck DJ. Cytokine regulation of skeletal muscle fatty acid metabolism: effect of interleukin-6 and tumor necrosis factor-alpha. Am J Physiol Endocrinol Metab 2004;287:E616–E621

26. Bruce CR, Risis S, Babb JR, et al. Overexpression of sphingosine kinase 1 prevents ceramide accumulation and ameliorates muscle insulin resistance in high-fat diet-fed mice. Diabetes 2012;61:3148–3155

27. McGee SL, Sadli N, Morrison S, Swinton C, Suphioglu C. DHA protects against zinc mediated alterations in neuronal cellular bioenergetics. Cell Physiol Biochem 2011;28:157–162
28. Lee-Young RS, Griffee SR, Lynes SE, et al. Skeletal muscle AMP-activated protein kinase is essential for the metabolic response to exercise in vivo. J Biol Chem 2009;284:23925–23934
29. Kim JK, Fillmore JJ, Sunshine MJ, et al. PKC-theta knockout mice are protected from fat-induced insulin resistance. J Clin Invest 2004;114:823–827
30. Koves TR, Ussher JR, Noland RC, et al. Mitochondrial overload and incomplete fatty acid oxidation contribute to skeletal muscle insulin resistance. Cell Metab 2008;7:45–56
31. Lin J, Handschin C, Spiegelman BM. Metabolic control through the PGC-1 family of transcription coactivators. Cell Metab 2005;1:361–370
32. Handschin C, Spiegelman BM. The role of exercise and PGC1alpha in inflammation and chronic disease. Nature 2008;454:463–469
33. Jäger S, Handschin C, St-Pierre J, Spiegelman BM. AMP-activated protein kinase (AMPK) action in skeletal muscle via direct phosphorylation of PGC-1alpha. Proc Natl Acad Sci U S A 2007;104:12017–12022
34. Kahn BB, Alquier T, Carling D, Hardie DG. AMP-activated protein kinase: ancient energy gauge provides clues to modern understanding of metabolism. Cell Metab 2005;1:15–25
35. Feige JN, Lagouge M, Canto C, et al. Specific SIRT1 activation mimics low energy levels and protects against diet-induced metabolic disorders by enhancing fat oxidation. Cell Metab 2008;8:347–358
36. Ruderman NB, Xu XJ, Nelson L, et al. AMPK and SIRT1: a long-standing partnership? Am J Physiol Endocrinol Metab 2010;298:E751–E760
37. Rodgers JT, Lerin C, Haas W, Gygi SP, Spiegelman BM, Puigserver P. Nutrient control of glucose homeostasis through a complex of PGC-1alpha and SIRT1. Nature 2005;434:113–118
38. Hoshino A, Mita Y, Okawa Y, et al. Cytosolic p53 inhibits Parkin-mediated mitophagy and promotes mitochondrial dysfunction in the mouse heart. Nat Commun 2013;4:2308
39. Palmer CS, Osellame LD, Stojanovski D, Ryan MT. The regulation of mitochondrial morphology: intricate mechanisms and dynamic machinery. Cell Signal 2011;23:1534–1545
40. Goto Y, Kakizaki M, Masaki N. Production of spontaneous diabetic rats by repetition of selective breeding. Tohoku J Exp Med 1976;119:85–90
41. Young JC, Hoogenraad NJ, Hartl FU. Molecular chaperones Hsp90 and Hsp70 deliver preproteins to the mitochondrial import receptor Tom70. Cell 2003;112:41–50
42. Leick L, Wojtaszewski JF, Johansen ST, et al. PGC-1alpha is not mandatory for exercise- and training-induced adaptive gene responses in mouse skeletal muscle. Am J Physiol Endocrinol Metab 2008;294:E463–E474
43. Rowe GC, El-Khoury R, Patten IS, Rustin P, Arany Z. PGC-1α is dispensable for exercise-induced mitochondrial biogenesis in skeletal muscle. PLoS One 2012;7:e41817
44. Morino K, Petersen KF, Sono S, et al. Regulation of mitochondrial biogenesis by lipoprotein lipase in muscle of insulin-resistant offspring of parents with type 2 diabetes. Diabetes 2012;61:877–887
45. Holloszy JO. Skeletal muscle "mitochondrial deficiency" does not mediate insulin resistance. Am J Clin Nutr 2009;89:463S–466S
46. Becker R, Laube H, Linn T, Damian MS. Insulin resistance in patients with the mitochondrial tRNA(Leu(UUR)) gene mutation at position 3243. Exp Clin Endocrinol Diabetes 2002;110:291–297
47. Reardon W, Ross RJ, Sweeney MG, et al. Diabetes mellitus associated with a pathogenic point mutation in mitochondrial DNA. Lancet 1992;340:1376–1379
48. Becker R, Laube H, Laube H, Linn T, Pabst W, Damian MS. Impaired glucose effectiveness in chronic progressive external ophthalmoplegia. Metabolism 2002;51:796–800
49. Linnane AW, Marzuki S, Ozawa T, Tanaka M. Mitochondrial DNA mutations as an important contributor to ageing and degenerative diseases. Lancet 1989;1:642–645
50. Trounce I, Byrne E, Marzuki S. Decline in skeletal muscle mitochondrial respiratory chain function: possible factor in ageing. Lancet 1989;1:637–639
51. Boffoli D, Scacco SC, Vergari R, Solarino G, Santacroce G, Papa S. Decline with age of the respiratory chain activity in human skeletal muscle. Biochim Biophys Acta 1994;1226:73–82
52. Cooper JM, Mann VM, Schapira AH. Analyses of mitochondrial respiratory chain function and mitochondrial DNA deletion in human skeletal muscle: effect of ageing. J Neurol Sci 1992;113:91–98
53. Safdar A, Bourgeois JM, Ogborn DI, et al. Endurance exercise rescues progeroid aging and induces systemic mitochondrial rejuvenation in mtDNA mutator mice. Proc Natl Acad Sci U S A 2011;108:4135–4140
54. Kuznetsov AV, Winkler K, Wiedemann FR, von Bossanyi P, Dietzmann K, Kunz WS. Impaired mitochondrial oxidative phosphorylation in skeletal muscle of the dystrophin-deficient mdx mouse. Mol Cell Biochem 1998;183:87–96
55. Millay DP, Sargent MA, Osinska H, et al. Genetic and pharmacologic inhibition of mitochondrial-dependent necrosis attenuates muscular dystrophy. Nat Med 2008;14:442–447
56. Gehrig SM, van der Poel C, Sayer TA, et al. Hsp72 preserves muscle function and slows progression of severe muscular dystrophy. Nature 2012;484:394–398